Facets and surface relaxation of tetrahexahedral platinum nanocrystals

Yong Ding, Yifan Gao, and Zhong Lin Wang[a)]
School of Materials Science and Engineering, Georgia Institute of Technology, Atlanta, Georgia 30332-0245, USA

Na Tian, Zhi-You Zhou, and Shi-Gang Sun
State Key Laboratory of Physical Chemistry of Solid Surfaces, Department of Chemistry, College of Chemistry and Chemical Engineering, Xiamen University, Xiamen 361005, China

(Received 1 August 2007; accepted 27 August 2007; published online 17 September 2007)

Platinum tetrahexahedral (THH) nanocrystals have been prepared by an electrochemical treatment of Pt nanospheres supported on glassy carbon by square-wave potential [N. Tian *et al.*, Science **316**, 732 (2007)]. In this paper, the shape and facets of the THH nanocrystals have been characterized by transmission electron microscopy. Most of the exposed surfaces are close to {730} facets. Detailed relaxation of the surface atoms has been observed at surface steps. It is anticipated that the high density of atomic steps and kinks is likely related to the enhanced catalytic activity of the THH nanocrystals. © *2007 American Institute of Physics*. [DOI: 10.1063/1.2785953]

In order to improve the catalytic activity of nanocrystals (NCs), besides the traditional method of reducing particle sizes, two major approaches have been taken: one is to choose bimetallic alloyed nanoparticles instead of elementary nanocrystals,[1] such as adding Ni into Pt to form Pt-alloyed nanoparticles,[2] and another is to modify the exposed surface to get higher concentration of atoms at the corners and edges.[3] For metallic NCs, it has been found that high Miller index planes, such as (210) and (410), generally exhibit much higher catalytic activity than that of the most common stable planes, such as {111} and {100}, because the high Miller index planes have a high density of atomic steps, ledges, and kinks, which usually serve as active sites for breaking chemical bonds.[4,5] In our previous work, we reported the synthesis of tetrahexahedral (THH) Pt NCs, which has a much improved electro-oxidation activity per surface area compared to the spherical Pt and the commercial Pt/C catalyst at room temperature.[6] As a continuation of this research, in this letter, we give the detailed electron microscopy characterization of the particle shape, facets, and surface relaxation of the THH Pt NCs. Our study will show the relaxation of surface atoms for the THH NCs.

The synthesis process of the THH NCs has been reported previously.[6] The THH Pt NCs were characterized by scanning electron microscope and high-resolution transmission electron microscopy at 400 kV using a JEM 4000EX. Our study relies on surface profile imaging for directly imaging the projection of surface atoms.[7–10] The shape of the Pt NC can be identified based on the information provided by scanning electron microscopy (SEM) and transmission electron microscopy (TEM) (Fig. 1). The clear edges of the particle shown in the SEM image [Fig. 1(a)] indicate that the particle looks like a cube with each face capped by a square-based pyramid, forming a THH. Figure 1(b) is a dark-field TEM image of a THH NC oriented with [001] parallel to the electron beam. The projected shape of the NC is clearly presented. Tilting the NC for 10° away from the [001] direction, another dark-field TEM image was acquired [Fig. 1(c)]. The fringes in the image are due to the variation of the projected thickness at different areas of the NC, which are called the thickness fringes. The shape of the NC can be marked in the image following the dashed lines. A three-dimensional (3D) model of the THH NC is presented in Fig. 1(d).

The shape of the NC can also be identified from a detailed analysis of the diffraction pattern. The selected-area electron diffraction (SAED) pattern shown in Fig. 2(a) was recorded from the Pt particle displayed in Fig. 1(b), which is the [001] zone-axis pattern of the face-centered-cubic structure. By carefully examining the diffraction spots, some fine features are found around each diffraction spot, especially for those with high indeces. These features are closely related to the shape of the NC.

From the electron diffraction theory,[11] exact Bragg diffracting condition is met when $\mathbf{u}=\mathbf{g}$, where $\mathbf{u}$ and $\mathbf{g}$ are the

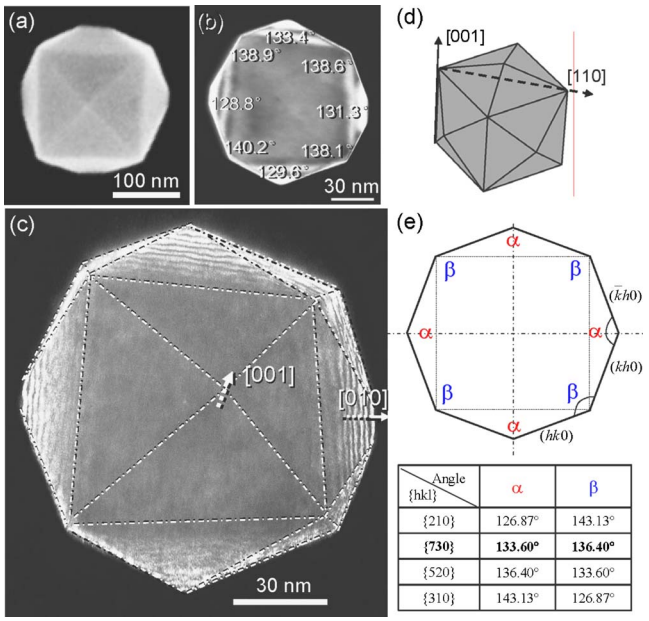

Angle {hkl}	α	β
{210}	126.87°	143.13°
{730}	**133.60°**	**136.40°**
{520}	136.40°	133.60°
{310}	143.13°	126.87°

FIG. 1. (Color online) (a) SEM image of a THH Pt nanocrystal and [(b) and (c)] two dark-field TEM images with incident electron beam along and ~10° away from the [001] direction, respectively. (d) Three-dimensional model of the THH Pt nanocrystal. (e) A two-dimensional projection draw of the THH nanocrystal and a table of the faceted angles calculated for the different surface planes.

[a)]Electronic mail: zlwang@gatech.edu and zhong.wang@mse.gatech.edu

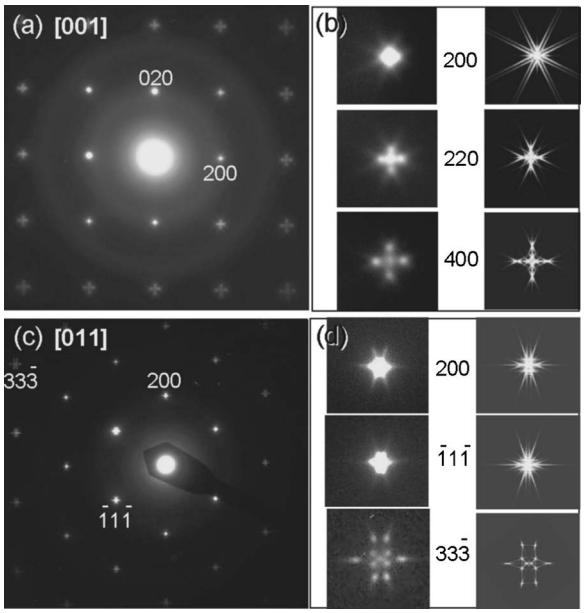

FIG. 2. [(a) and (c)] SAED patterns recorded from Pt NC with electron beam along [001] and [011], respectively. (b) and (d) show the corresponding enlarged experimental diffraction spots (left) and the simulated results (right).

reciprocal space vector and reciprocal lattice vector, respectively. However, due to the finite size of a crystal, there has an intensity distribution around **g** (**u**=**g**+**s**, where **s** is the excitation error in electron diffraction) as defined by a shape factor, which is a 3D Fourier transform of the crystal volume:

$$\phi_g = \frac{1}{V_c}\int_{crystal} \exp(-2\pi isr)d\tau, \tag{1}$$

where V_c is the volume of the unit cell. The diffraction intensity is $\phi_g\phi_g^*$. Considering the geometry of electron diffraction, the intensity recorded in diffraction pattern is an intersection of the Ewald sphere with the shape factor. In the two-dimensional (2D) zone-axis diffraction pattern, the excitation error gradually increases with the increase of scattering angle. Although the intensity distribution around each reciprocal lattice is the same in 3D, the recorded intensities of the diffraction spots in 2D zone-axis diffraction pattern will be different due to the different excitation errors for diffraction spots. Further, due to the diffraction spots nearby the center beam, which are close to the Bragg's condition, the strong diffraction at reciprocal lattice point shadows the fine features introduced by the shape factor. Therefore, the shape factor introduced intensity distribution can be seen more clearly around the high-indexed diffraction spots.

In order to use the fine features observed around the diffraction spots in Fig. 2(a) to refine the shape of the NC, we have carried out some calculations using Eq. (1). The enlarged experimental data (left) and calculated results (right) are displayed in Fig. 2(b). Based on the information supplied by the dark-field images in Fig. 1, we assume the shape of the particle as THH. The excitation error **s** was determined using the Ewald sphere for 400 kV electrons for [001] incident beam direction for the case of Pt. The particle size can be measured directly from the TEM images displayed in Fig. 1(b). To make the best fit, we tried the cases of surface facets being {110}, {210}, {310}, {520}, and {730}. The different exposed surfaces show different streaking orientations around the diffraction spots, as shown in Figs. 2(a) and 2(b). Compared to the experimental data, the best matched result is the shape enclosed by the {730} facets.

The diffraction pattern shown in Fig. 2(c) was recorded from the Pt NC with the incident beam along the [011] orientation. The enlarged experimental data (left) and the calculated results (right) are displayed in Fig. 2(d). The calculation was based on the same THH shape. The asymmetrical intensity distribution of **g** and **−g** in the diffraction pattern of Fig. 2(c) is due to a small angle deviation from the right zone axis, but it does not affect the detailed shape factor introduced intensity distribution around each diffraction spot.

The Miller indices of the surface facets can be determined either by TEM images combined with diffraction pattern or by high-resolution transmission electron microscopy (HRTEM) images. With the incident electron beam parallel to the [001] direction, the side facets of the THH nanocrystals are imaged edge on in the recorded TEM images, like the cases shown in Fig. 1(b). The ideal project shape of a THH NC should look like the sketch drawn in the upper part of Fig. 1(e). The Miller indices of the edge-on facets of the THH can be identified by a conjunction of the angles between the facets. For the eight edge-on facets parallel to the [001] zone axis, they can be indexed as {*hk*0}. The two ideal angles α and β that correspond to different Miller indices are listed in the bottom chart of Fig. 1(e). The measured surface angles α and β of the Pt nanocrystals are marked in Fig. 1(b). It can be found that the angle α is between 126.87° and 133.60°, while angle β is between 143.13° and 136.40°. Therefore, the facets are high Miller index surfaces, most close to {730}, which is consistent to our result derived from the shape factor, as shown in Fig. 2.

The HRTEM image of one such as high Miller index facet is displayed in Fig. 3(a), which was recorded along [001]. The projected atom positions at the edges of the surface steps are clearly seen, with some of the atoms being relaxed outward, as indicated by arrowheads. To quantify the position of the projected atom positions, the centers of the projected atom columns are marked by + [Fig. 3(b)]. The high Miller index surface consists of (100) terraces separated by atomic steps. If we follow the nomenclature for ordered stepped surfaces by Blakely and Somorjai,[12] the Pt surface composed by a (100) terrace with *m* atomic rows and (010) step with *n* atom height can be presented as $[m(100)\times n(010)]$. Then, the (110), (210), and (310) facets can be described as $(100)\times(010)$, $2(100)\times(010)$, and $3(100)\times(010)$, respectively. While (730) facet corresponds to the periodically stacking of two $2(100)\times(010)$ and one $3(100)\times(010)$. Examining the surface in Fig. 3(a) carefully, we can find that it is consisted of a series of (110), (210), and (310) facets although the entire profile is close to the (730) facet.

Our previous property measurements show that THH Pt NCs exhibit much enhanced catalytic activity per unit surface area than the spherical particles for the oxidation of small organic molecules.[6] This may be attributed to the high density of steps on the surfaces of THH Pt NCs. The unreconstructed (110) facets have the highest density of steps, as displayed in Fig. 3(c), because all of the surface atoms are on the step. However, the (110) surface usually has a 1×2 reconstruction [as shown in Fig. 3(c) omitting the dashing bonds],[13] sometimes even 1×3 or 1×5 reconstruction.[14] There are only one-third of surface atoms located on the step

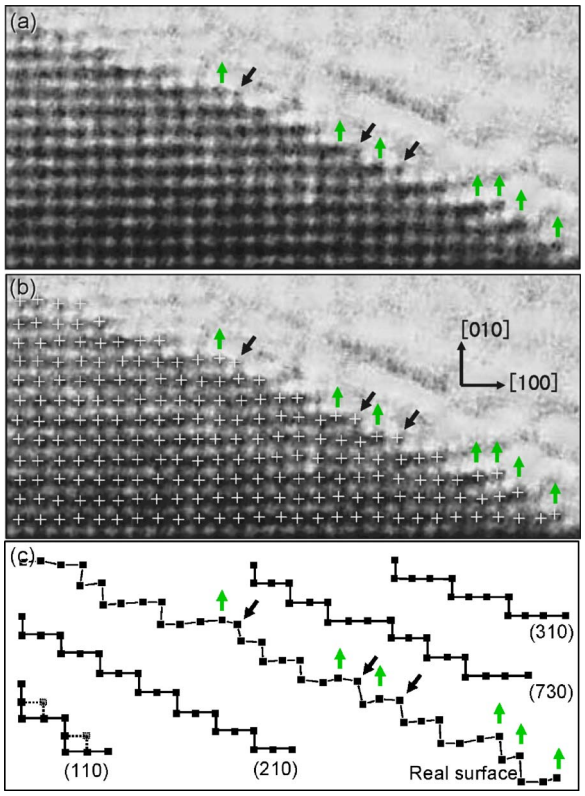

FIG. 3. (Color online) (a) HRTEM image of one surface facet of THH Pt NC, and (b) is a duplication of (a) with the center of each atom column marked by "+." (c) The step configurations of (110), (210), (730), (310), and the real surfaces received from (b).

in the 1×2 reconstructed (110) facet. Examining the surface atoms on the (210), (310), and (730) facets, we can found that 1/2, 1/3, and 3/7 of the surface atoms are on the steps, respectively. The real facet observed in Fig. 3(a) has ~46% surface atoms located at the steps, which is between those for the (210) and (730) facets.

The HRTEM image in Fig. 3(a) also contains the relaxation information of surface atoms. The identification of the atom centers (dark contrast centers) makes the quantity measurement of the displacement of surface atoms possible. If we take the coordinate system as shown in Fig. 3(b), two major types of relaxation can be identified. One is along the $[\bar{1}\bar{1}0]$ direction as indicated by dark arrowheads, with an inward displacement as large as $10\%a$, where a is the lattice parameter of Pt unit cell; another is dominated in the [010] direction as indicated by green arrowheads, with an outward displacement normally below $7\%a$.

The atoms taking $[\bar{1}\bar{1}0]$ inward displacement are located at the step sites and show comparably light-contrast, which indicates their lower site occupancy. It is more precise to call these locations as ledges or kinks instead of steps. At these locations, the coordination is much lower than those located at a step, terrace, and bulk. The inward movement along the $[\bar{1}\bar{1}0]$ direction, if possible, combined with the displacement along the [001] direction (which cannot be identified in the HRTEM image shown in Fig. 3), tend to increase the coordination of the surface atoms.

High percentages of the atoms taking [010] outward displacement are located at the terraces and next to the step atoms. They have comparably higher atomic coordination than those of step, kink, and ledge atoms; therefore, their comparably small [010] displacement is reasonable. Some of them also show the displacement along the $[\bar{1}00]$ direction, but the amplitude is smaller than that in the [010] direction. Noticeably, there have some step atoms at the right-bottom side of the HRTEM image in Fig. 3(b) also taking [010] instead of $[\bar{1}\bar{1}0]$ inward displacement. Based on their contrast, we can find that they are well occupied atomic columns as those at terraces. Our observation of the surface relaxation is consistent with the theoretical calculation of the missing row surface reconstruction.[15]

In summary, the tetrahexaheral shape of the Pt nanocrystals has been identified by dark-field TEM images, the shape factor observed in electron diffraction patterns, and HRTEM. Most of the exposed facets are belonging to the {730} family planes. Significant surface relaxation has been observed for the atoms at the surface steps on {730}. The existence of high density of steps and kinks (and/or ledges) at the surface is likely to be responsible to the enhanced catalytic activity.

Y.D., Y.F.G., and Z.L.W. thank the support from US NSF and DOE (BES, DE-FG02-07ER46394). N.T., Z.Y.Z., and S.G.S. thank the support from NSFC (20433060, 20503023, and 20673091) and Special Funds for Major State Basic Research Project of China (2002CB211804).

[1] G. F. Wang, M. A. Van Hove, P. N. Ross, and M. I. Baske, Prog. Surf. Sci. **79**, 28 (2005).
[2] V. R. Stamenkovic, B. S. Mun, M. Arenz, K. J. J. Mayrhofer, C. A. Lucas, G. F. Wang, P. N. Ross, and N. M. Markovic, Nat. Mater. **6**, 241 (2007).
[3] R. Narayanan and M. A. El-Sayed, Nano Lett. **4**, 1343 (2004).
[4] N. Hoshi, S. Kawatani, M. Kudo, and Y. Hori, J. Electroanal. Chem. **467**, 67 (1999).
[5] S. G. Sun and J. Clavilier, Chem. J. Chin. Univ. **11**, 998 (1990).
[6] N. Tian, Z. Y. Zhou, Y. Ding, and Z. L. Wang, Science **316**, 732 (2007).
[7] D. A. Jefferson and P. J. Harris, Nature (London) **332**, 617 (1988).
[8] L. D. Marks and V. Heine, Phys. Rev. Lett. **52**, 656 (1984).
[9] L. D. Marks, Rep. Prog. Phys. **57**, 603 (1994).
[10] Y. Ding and Z. L. Wang, Surf. Sci. **601**, 425 (2007).
[11] Z. L. Wang, *Elastic and Inelastic Scattering in Electron Diffraction and Imaging* (Plenum, New York, 1995), Chap. 1, pp. 3–21.
[12] D. W. Blakely and G. A. Somorjai, Surf. Sci. **65**, 419 (1977).
[13] L. D. Marks, Phys. Rev. Lett. **51**, 1000 (1983).
[14] I. K. Robinson, M. C. Saint-Lager, P. Dolle, S. Boutet, M. De Santis, and R. Baudoing-Savois, Surf. Sci. **575**, 321 (2005).
[15] S. Olivier, G. Tréglia, A. Saúl, and F. Willaime, Surf. Sci. **600**, 5131 (2006).